

REPORT DOCUMENTATION PAGE			Form Approved OMB NO. 0704-0188		
<p>The public reporting burden for this collection of information is estimated to average 1 hour per response, including the time for reviewing instructions, searching existing data sources, gathering and maintaining the data needed, and completing and reviewing the collection of information. Send comments regarding this burden estimate or any other aspect of this collection of information, including suggestions for reducing this burden, to Washington Headquarters Services, Directorate for Information Operations and Reports, 1215 Jefferson Davis Highway, Suite 1204, Arlington VA, 22202-4302. Respondents should be aware that notwithstanding any other provision of law, no person shall be subject to any penalty for failing to comply with a collection of information if it does not display a currently valid OMB control number.</p> <p>PLEASE DO NOT RETURN YOUR FORM TO THE ABOVE ADDRESS.</p>					
1. REPORT DATE (DD-MM-YYYY)		2. REPORT TYPE		3. DATES COVERED (From - To)	
		New Reprint		-	
4. TITLE AND SUBTITLE Computational investigation of structured shocks in Al/SiC-particulate metal-matrix composites			5a. CONTRACT NUMBER		
			W911NF-09-1-0513		
			5b. GRANT NUMBER		
6. AUTHORS M. Grujicic, W.C. Bell, B. Pandurangan, C.-F. Yen, B.A. Cheeseman			5c. PROGRAM ELEMENT NUMBER		
			622105		
			5d. PROJECT NUMBER		
			5e. TASK NUMBER		
			5f. WORK UNIT NUMBER		
7. PERFORMING ORGANIZATION NAMES AND ADDRESSES			8. PERFORMING ORGANIZATION REPORT NUMBER		
Clemson University Office of Sponsored Programs 300 Brackett Hall Clemson, SC 29634 -5702					
9. SPONSORING/MONITORING AGENCY NAME(S) AND ADDRESS(ES) U.S. Army Research Office P.O. Box 12211 Research Triangle Park, NC 27709-2211			10. SPONSOR/MONITOR'S ACRONYM(S) ARO		
			11. SPONSOR/MONITOR'S REPORT NUMBER(S) 56526-EG.11		
12. DISTRIBUTION AVAILABILITY STATEMENT Approved for public release; distribution is unlimited.					
13. SUPPLEMENTARY NOTES The views, opinions and/or findings contained in this report are those of the author(s) and should not be construed as an official Department of the Army position, policy or decision, unless so designated by other documentation.					
14. ABSTRACT Propagation of planar (i.e. one directional), longitudinal (i.e. uniaxial strain), steady (i.e. time-invariant) structured shock waves within metal matrix composites (MMCs) is studied computationally. Waves of this type are typically generated during blast-wave loading or ballistic impact and play a major role in the way blast/ballistic impact loads are introduced in, and applied to, a target structure. Hence, the knowledge of the basic physics of propagation of these waves is critical for designing structures with superior blast and impact protection capabilities. To derive the					
15. SUBJECT TERMS Aluminium, Composite materials, Wave propagation, Mechanical shock, Metal matrix composites, Structured shocks, Dynamic mixture model					
16. SECURITY CLASSIFICATION OF:			17. LIMITATION OF ABSTRACT	15. NUMBER OF PAGES	19a. NAME OF RESPONSIBLE PERSON
a. REPORT	b. ABSTRACT	c. THIS PAGE			Mica Grujicic
UU	UU	UU	UU		19b. TELEPHONE NUMBER
					864-656-5639

## Report Title

Computational investigation of structured shocks in Al/SiC-particulate metal-matrix composites

### ABSTRACT

Propagation of planar (i.e. one directional), longitudinal (i.e. uniaxial strain), steady (i.e. time-invariant) structured shock waves within metal matrix composites (MMCs) is studied computationally. Waves of this type are typically generated during blast-wave loading or ballistic impact and play a major role in the way blast/ballistic impact loads are introduced in, and applied to, a target structure. Hence, the knowledge of the basic physics of propagation of these waves is critical for designing structures with superior blast and impact protection capabilities. To derive the overall response of the composite material to shock type loading, a dynamic-mixture model is employed. Within this model, the known constitutive responses of the constituent materials are combined using the appropriate mixture rules. These mixture rules are of a dynamic character since they depend on the current state of the composite material and cannot be applied prior to the beginning of the analysis.

The approach is applied to a prototypical MMC consisting of an aluminum matrix and SiC particulates. Both the intermediate-to-strong shock regime (in which the contribution of stress deviators to the stress field can be ignored) and the weak shock regime (in which stress deviators provide a significant contribution to the stress field) are investigated. Finally, the computational results are compared with their experimental counterparts available in the open literature in order to validate the computational procedure employed.



---

**REPORT DOCUMENTATION PAGE (SF298)**  
**(Continuation Sheet)**

---

Continuation for Block 13

ARO Report Number 56526.11-EG  
Computational investigation of structured shocks ...

Block 13: Supplementary Note

© 2011 . Published in Multidiscipline Modeling in Materials and Structures, Vol. Ed. 0 7, (4) (2011), (, (4). DoD Components reserve a royalty-free, nonexclusive and irrevocable right to reproduce, publish, or otherwise use the work for Federal purposes, and to authorize others to do so (DODGARS §32.36). The views, opinions and/or findings contained in this report are those of the author(s) and should not be construed as an official Department of the Army position, policy or decision, unless so designated by other documentation.

Approved for public release; distribution is unlimited.



# Computational investigation of structured shocks in Al/SiC-particulate metal-matrix composites

Structured  
shocks in MMCs

469

M. Grujicic, W.C. Bell and B. Pandurangan  
*Department of Mechanical Engineering, Clemson University,  
Clemson, South Carolina, USA, and*  
C.-F. Yen and B.A. Cheeseman  
*Survivability Materials Branch, Army Research Laboratory,  
Aberdeen, Maryland, USA*

Received 14 April 2010  
Accepted 10 June 2011

## Abstract

**Purpose** – Propagation of planar (i.e. one directional), longitudinal (i.e. uniaxial strain), steady (i.e. time-invariant) structured shock waves within metal matrix composites (MMCs) is studied computationally. Waves of this type are typically generated during blast-wave loading or ballistic impact and play a major role in the way blast/ballistic impact loads are introduced in, and applied to, a target structure. Hence, the knowledge of the basic physics of propagation of these waves is critical for designing structures with superior blast and impact protection capabilities. The purpose of this paper is to help advance the use of computational engineering analyses and simulations in the areas of design and application of the MMC protective structures.

**Design/methodology/approach** – To derive the overall response of the composite material to shock type loading, a dynamic-mixture model is employed. Within this model, the known constitutive responses of the constituent materials are combined using the appropriate mixture rules. These mixture rules are of a dynamic character since they depend on the current state of the composite material and cannot be applied prior to the beginning of the analysis.

**Findings** – The approach is applied to a prototypical MMC consisting of an aluminum matrix and SiC particulates. Both the intermediate-to-strong shock regime (in which the contribution of stress deviators to the stress field can be ignored) and the weak shock regime (in which stress deviators provide a significant contribution to the stress field) are investigated. Finally, the computational results are compared with their experimental counterparts available in the open literature in order to validate the computational procedure employed.

**Originality/value** – Prediction of the spallation-type failure in a metal-matrix composite material (modeled using the dynamic-mixture model) has not been done previously.

**Keywords** Aluminium, Composite materials, Wave propagation, Mechanical shock, Metal matrix composites, Structured shocks, Dynamic mixture model

**Paper type** Research paper



The material presented in this paper is based on work supported by the Army Research Office (ARO) research contract entitled “Multi-length Scale Material Model Development for Armor-grade Composites”, Contract Number W911NF-09-1-0513, and the Army Research Laboratory (ARL) research contract entitled “Computational Analysis and Modeling of Various Phenomena Accompanying Detonation Explosives Shallow-Buried in Soil” Contract Number W911NF-06-2-0042.

## 1. Introduction

Owing to their ability to simultaneously satisfy a variety of manufacturing/processing constraints and functional/performance requirements (via material property tailoring), advanced metal-matrix composites (MMCs) are increasingly being used in a variety of applications. Among these applications are the ones in automotive-engineering (e.g. crash-worthy structures), aerospace industry (e.g. space debris impact shields) and defense industry (e.g. light-weight, high-performance blast and ballistic protection systems) (Pandey *et al.*, 2001). In these applications, full advantage is taken of the superior performance of MMCs under high loading-rate conditions. It is generally recognized that in order to further increase the performance of MMCs in the high loading-rate applications, improved knowledge of the basic physics related to shock-wave generation and propagation (addressed in the present work) and the associated micro-structure evolution and material deformation/degradation processes (to be addressed in our future work) is required.

It is generally recognized that any analysis of the shock-wave generation and propagation phenomena within MMCs and the associated micro-structure evolution and material deformation/degradation processes must include the consideration of the following specific aspects of this class of materials:

- These materials are heterogeneous and consist of at least two phases: a metallic matrix and (typically ceramic) reinforcements. In addition, these materials often contain (undesirable) voids (and perhaps other defects/flaws). The MMCs analyzed in the present work are assumed to be free of voids and other flaws.
- These materials may be associated with different levels of (micro-structure and processing-induced) elastic and/or inelastic anisotropies. The class of MMCs selected for analysis in the present manuscript is typically considered to be elastically and inelastically isotropic.
- Properties of the MMCs are not only controlled by the relative amounts, micro-structure/morphology and properties of the constituent materials but also by the constitutive properties of the matrix/reinforcement interphases. Owing to the fact that strong matrix/reinforcement bonding can be achieved through proper sizing treatment of the reinforcement in the class of MMCs analyzed and that only the response of these materials to compressive shocks was investigated, perfect bonding is assumed to exist at the matrix/reinforcement interfaces.

The development of advanced MMC-based protective (i.e. blast-survivable and ballistic-resistant) structures with superior performance typically involves extensive application of the experimental test procedures/programs. Such experimental test programs are critical for ensuring the utility and effectiveness of the composite-material protective structures. However, this approach is often associated with a prohibitively high cost and involves destructive (one-shot) testing. While the role of experimental test programs remains critical, they are increasingly being complemented by the corresponding computation-based engineering analyses and simulations. The knowledge of composite-material response under various in-service loading conditions, as described by the corresponding material model(s), is one of the key components in such analyses greatly affecting their utility and fidelity. The main objective of the present work is to help advance the use of these computational engineering analyses and simulations in the areas of design and application of the MMC

---

protective structures. Towards that end, high loading-rate constitutive models for a class of MMCs is developed and implemented (via a user-material subroutine) into a commercial finite-element program.

Examination of the public-domain literature carried out here in revealed a large number of (mainly static) material models for the MMCs. These models can be classified in a variety of ways. For example, the micro-structure length scale which is being emphasized in the model can be used for the MMC-material model classification. This classification typically yields the following classes of MMC-material models: continuum length-scale (Lee *et al.*, 2009), grain-size length-scale (Abu Al-Rub, 2009) and atomistic length-scale (Dang and Grujicic, 1997). Alternatively, MMC-material models can be classified according to the morphology (and size) of the reinforcements as whiskers-reinforced MMCs (Davis, 1993), particulate-reinforced MMCs (Hunt *et al.*, 1990), dispersion-reinforced MMCs (Davis, 1997), etc.

The classification of the MMC-material models employed in the present work is based on the loading-rate range at which the model is applicable. Consequently, and for simplicity, the MMC-material models are classified into two groups as:

- (1) those applicable under quasi-static and/or sub-sonic dynamic deformation rate conditions (Li *et al.*, 2007); and
- (2) those applicable under super-sonic (i.e. shock-wave) loading conditions (Vecchio and Gray, 1994).

While there are material models in the literature which retain the discrete nature of the two MMC-material components (i.e. of the metallic matrix and the discrete reinforcements), the ones considered in the present work treat the MMC as a homogenized/smeared-out mixture of the two components. The main reason for this is that the interest of the present work was into MMC-material models which are suitable for large-scale computational investigations of the blast/ballistic survivability of MMC protective structures (e.g. vehicle underbody armor). In these investigations, due to a prohibitively high computational cost, one cannot afford to treat the MMC material as a heterogeneous two-component medium, but is forced to consider the same as a homogenized/smeared-out “single-component” material. However, as will be discussed later the two-phase nature of the MMC is not completely discounted since the effective response of the smeared-out composite material is obtained dynamically from the responses of the individual constituents.

Careful examination of the material models falling into the two classes adopted in the present work revealed that the models differ generally in the way the two components are mixed/homogenized. In other words, different assumptions are involved regarding partitioning of stresses and strains between the matrix and the reinforcements. In majority of the material models, the volume fractions of the MMC-material components are assumed to remain unchanged during loading/deformation. While this assumption appears justifiable in the case of quasi-static and sub-sonic dynamic loading conditions (which are associated with relatively small volumetric strains), the same cannot be stated in the case of shock-wave loading (a type of loading which is dominated by the spherical/hydrodynamic component of the stress tensor and may result in large volumetric strains). Consequently, as will be discussed in greater detail in next section, under dynamic loading, the volume fractions of the MMC components have to be treated as material-state variables whose values depend on the state of loading of the MMC as well as on the constitutive response of the constituents at a given material point.

---

In the present work, an attempt is made to further advance the MMC-material model derived in our previous work (Grujicic *et al.*, 2011a). This model is based on the so-called “dynamic-mixture” material model originally proposed by Drumheller (1987) and Anderson *et al.* (1990). The model was aimed at capturing the effective response of MMCs when subjected to shock-wave loading in the intermediate to strong shock regime (within which the material stress field is dominated by its spherical/hydrodynamic component). The model is of a homogenization-type, i.e. each material point is assumed to contain both of the MMC components. The model also assumed that there is no relative motion between the two constituents residing at a given material point resulting in constancy of the constituent (local) mass fractions. On the other hand, as mentioned above, the constituent volume fractions are treated as (evolving) material – state variables. As will be shown later, the evolution of the constituent volume fractions during loading are obtained by solving simultaneously, at each time step, a set of equations consisting of the governing (mass, linear momentum and energy) conservation/balance equations, constituent constitutive relations and the appropriate mixture-rule relations.

In the present work, an attempt is made to extend our recently developed MMC dynamic-mixture-based material model in two ways (Grujicic *et al.*, 2011a):

- (1) In the intermediate to strong shock regime, in addition to the adiabatic limit (analyzed in Grujicic *et al.*, 2011a), the isothermal limit is also investigated. The adiabatic and isothermal limits correspond to the cases of total absence and complete thermal-energy exchange between the MMC constituents residing at the same material point during high-rate loading.
- (2) The shock propagation is also analyzed in the weak-shock regime (in which the contribution of the stress deviators and inelastic deformation processes to the material state must be accounted for).

The organization of the paper is as follows: a critical review of the dynamic-mixture model and the application of this model to a prototypical isotropic two-constituent MMC (a silicon carbide particulate-reinforced aluminium-matrix composite) is provided in Section 2. The main results obtained are presented and discussed in Section 3 while the conclusions resulting from the present study are summarized in Section 4.

## 2. Overview of the dynamic-mixture theory

### 2.1 A critical overview

In this section, a brief critical overview is provided of the dynamic-mixture composite-material model originally developed by Drumheller (1987) and Anderson *et al.* (1990). As mentioned earlier, this is an example of a homogenization composite-material model, within which each material point is assumed to contain all the constituent phases of the material and the properties/responses of the composite materials are derived through proper mixing of the constituent properties/responses. However, constituent mixing is carried out dynamically, i.e. using rule of mixtures which depend on the current state of the material. In other words, the constituent volume fractions are not considered as constant but rather treated as dynamic, solution-dependent variables. It should be noted that while the dynamic-mixture theory is applicable to a general non-reactive, multi-constituent system, only a binary (two constituent) rendition of this theory is analyzed henceforth.

The transient non-linear dynamic response of composite materials (or materials, in general) is governed by the mass, momentum and energy conservation equations. The dynamic-mixture theory has been developed with the recognition that within standard commercial transient non-linear dynamics codes, user modifications to the mass and momentum conservation equations are typically not permitted. Instead, the user is allowed to provide/implement the appropriate material constitutive relations as well as to assess various components of the internal-energy density.

*Mass conservation equation.* In acknowledging the aforementioned limitations of the commercial codes and recognizing that within the extremely short time associated with shock-wave loading relative motion between the constituents associated with a single material point can be neglected (i.e. particle velocities for the constituents associated with the same material point are assumed to be equal), the dynamic-mixture theory preserves the original (single-constituent) form of the mass and the linear momentum conservation equations as:

$$\dot{\rho} + \rho \frac{\partial \dot{x}_\alpha}{\partial x_\alpha} = 0 \quad (1)$$

$$\rho \ddot{x}_\alpha = - \frac{\partial}{\partial x_\alpha} (P + Q) + \rho f_\alpha + \frac{\partial S_{\beta\alpha}}{\partial x_\beta} \quad (2)$$

where  $\rho$  is the material mass-density,  $f$  is the mass-based body-force,  $x_\alpha$  the  $\alpha$ -th spatial coordinate,  $\dot{x}_\alpha$   $\alpha$ -th component of the particle velocity (defined as a time derivative of the particle spatial coordinates) and  $S_{\beta\alpha}$  are the components of the stress deviator. The summation convention is implied by the repeated subscripts  $\alpha, \beta = 1, 2, 3$ . The raised dot denotes a material derivative ( $= \partial/\partial t + \partial/\partial x_\alpha \dot{x}_\alpha$ ).  $P$  is the (equilibrium/physical) pressure and  $Q$  is the dissipative-pressure. It should be noted that all the quantities appearing in equations (1) and (2) pertain to the composite material and are obtained (as will be shown below) through proper mixing of the respective constituent properties. Among the constituent properties (state variables) which define the constitution/make-up of the composite material are:

- intrinsic mass density of each component,  $\bar{\rho}_\varepsilon, \quad \varepsilon = 1, 2;$
- volume fraction of each component,  $\phi_\varepsilon, \quad \varepsilon = 1, 2;$
- partial density of each component,  $\rho_\varepsilon, \quad \varepsilon = 1, 2;$  and
- (constant) mass fraction of each component,  $M_\varepsilon, \quad \varepsilon = 1, 2.$

These state variables are not all independent but rather are related through the following set of equations:

$$\sum_\varepsilon \phi_\varepsilon = 1, \quad \sum_\varepsilon M_\varepsilon = 1 \quad (3)$$

$$\rho_\varepsilon = \phi_\varepsilon \bar{\rho}_\varepsilon \quad (4)$$

$$\rho = \sum_\varepsilon \rho_\varepsilon \quad (5)$$

$$M_\varepsilon = \frac{\rho_\varepsilon}{\rho} \quad (6)$$

Combining equations (4) and (6) yields:

$$\bar{\rho}_1 = \frac{M_1 \rho}{\phi_1} \quad (7)$$

$$\bar{\rho}_2 = \frac{M_2 \rho}{\phi_2} = \frac{(1 - M_1) \rho}{1 - \phi_1} \quad (8)$$

It should be noted that equations (3)-(8) relate the composite-material mass-density (used in the mass and momentum conservation equations, equations (1) and (2)) to the constituent volume-fractions and mass-densities. Alternatively, if the composite density is known, the knowledge of one of the constituent volume fractions or densities is required to obtain the remaining constituent volume fractions and densities. It should be also recognized that the constant mass-fraction condition is a direct consequence of the assumed absence of relative motion between the constituents.

*Momentum conservation equation.* To relate the composite-material total pressure (used in the momentum conservation equation, equation (2)) with the constituents' total pressure, the following pressure-mixing relation is used:

$$P + Q = P_\varepsilon + Q_\varepsilon, \quad (\varepsilon = 1, 2) \quad (9)$$

where the quantities without subscripts pertain to the composite material, while the quantities with subscripts pertain to the individual constituents.

One can next use a simple thought experiment to demonstrate that the pressure-equality condition defined by equation (9) makes the constituent volume fractions  $\phi_\varepsilon$  non-constant. One should begin by considering a single cube-shaped computational-cell which contains the two constituents at equal (0.5) volume fractions. Next, it is postulated that each of the two constituents resides within their respective computational sub-cell with constituent interface being parallel with one of the faces of the cube. The cube is next subjected to uniaxial-strain loading in a direction parallel with the inter-component boundary. To satisfy the equal-pressure condition, the stiffer constituent must undergo a smaller volume change than the more compliant one. However, since both constituents are subjected to the same uniaxial-strain, this could be accomplished only if the components experience an additional normal strain in a direction normal to the constituent interface. The latter strain would then give rise to a change in the volume fractions of the components. It should be recalled that while the volume fractions of the two components may change under dynamic loading, the corresponding mass-fractions remain constant.

According to equation (9), the total pressure for the composite material (used in the momentum conservation equation (2)) can be evaluated by computing the corresponding quantity for one of the constituents. The constituent equilibrium pressure is typically defined in terms of an equation of state (EOS) in the form:

$$P_\varepsilon = \hat{P}_\varepsilon(\bar{\rho}_\varepsilon, \bar{E}_\varepsilon) \quad (10)$$

while the constituent dissipative pressure is typically defined using a viscous-damping relation in the form:

$$Q_\varepsilon = \hat{Q}_\varepsilon(\bar{\rho}_\varepsilon, \dot{\bar{\rho}}_\varepsilon) \quad (11)$$

where  $\bar{E}_\varepsilon$  is the intrinsic mass-based energy density of the  $\varepsilon$ -th constituent (i.e. the internal energy associated with constituent  $\varepsilon$  per unit mass of the same constituent).

As far as the stress deviator  $S_{\alpha\beta}$  is concerned, it is assumed, as will be discussed in Appendix 1, to be controlled by the composite-material effective shear modulus and the composite-material deviatoric strain. Owing to the absence of relative motion of the constituents residing within the same material point, the composite-material effective shear modulus is assumed to be defined by an equal-strain rule of mixture.

*Energy conservation equation.* Within the dynamic-mixture model, the composite-material energy conservation equation is handled in the following way:

- First the corresponding energy conservation equations are defined/evaluated for the two constituents as:

$$\rho_\varepsilon \dot{\bar{E}}_\varepsilon = \phi_\varepsilon (P_\varepsilon + Q_\varepsilon) \frac{\dot{\rho}_\varepsilon}{\rho_\varepsilon} + \rho_\varepsilon r_\varepsilon + \rho_\varepsilon \dot{\bar{E}}_\varepsilon^d, \quad (\varepsilon = 1, 2) \quad (12)$$

where  $r_\varepsilon$  is the constituent intrinsic mass-based internal-power density source/sink term and  $\dot{\bar{E}}_\varepsilon^d$  is the constituent mass-based distortional power density (discussed in greater detail in Appendix 1).

- The composite-material energy-density is next defined using the following energy-mixing relation as:

$$\rho E = \sum \rho_\varepsilon \bar{E}_\varepsilon, \quad (\varepsilon = 1, 2) \quad (13)$$

In regard to computation of the constituent energy-density as defined by equation (12), Drumheller (1987) and Anderson *et al.* (1990) considered two limiting cases:

- (1) an adiabatic case; and
- (2) an isothermal case.

In the adiabatic case, the two composite-material constituents residing at the same material point are not allowed to exchange their thermal/internal energies. Consequently, for each constituent the mass-based internal-power density source/sink term  $r_\varepsilon$  in equation (12) is set to zero.

In the isothermal case, on the other hand, the two composite-material constituents residing at the same material point are allowed to fully exchange their thermal/internal energies until the thermal equilibrium (equal temperature,  $T_1 = T_2$ ) condition, in the form:

$$\frac{\bar{E}_1}{(C_p)_1} = \frac{\bar{E}_2}{(C_p)_2}, \quad (14)$$

is met, where  $C_p$  denotes the mass-based, constant-pressure specific heat. In this case, equation (12) contains non-zero  $r_\varepsilon$  terms but  $r_1 = -r_2$  (to account for the fact that the energy-density sink/source term is associated with a thermal-energy exchange between the constituents residing at the same material point). The sink/source term appearing in equation (12) can be evaluated through the use of the equal-temperature condition (equation (14)).

As far as the constituent distortional power/energy terms are concerned, as will be discussed in greater detail in Appendix 1, these quantities are evaluated by

partitioning the composite-material distortional power/energy (evaluated from the known composite-material deformation gradient) in accordance with the total internal-energy density partitioning (equation (13)).

*Dependent variables and governing equations.* To help identify the dependent variables and the associated governing equations, the case of uniaxial motion in the  $x_1$  direction is first considered here. In this case, the composite-material deviatoric-strain component can be directly related to the current (known) density and the deviatoric stress  $S_{11}$  can be directly calculated. Hence, in this case, there are nine dependent variables:  $P_1, Q_1, \bar{\rho}_1, \bar{E}_1, P_2, Q_2, \bar{\rho}_2, \bar{E}_2$  and one of the composite-material constitution variables (e.g.  $\phi_1$ ). The associated nine equations are as follows:

- (1)  $P_1$  and  $P_2$  are defined by the respective two EOS relations in accordance with equation (10).
- (2)  $Q_1$  and  $Q_2$  are defined by the respective two viscous dissipation relations in accordance with equation (11).
- (3)  $\bar{\rho}_1$  and  $\bar{\rho}_2$  are defined by equations (7) and (8).
- (4)  $\bar{E}_1$  and  $\bar{E}_2$  are defined by the respective two energy conservation equations in accordance with equation (12) (and equation (14), in the case of isothermal energy-mixing rule).
- (5)  $\phi_1$  is calculated using the total pressure-equality relation, equation (9). It should be noted that, the distortional-energy terms  $\Delta E_e^d$  are not counted as independent variables. This is done so because, as will be shown in Appendix 1, these constituent distortional energies are directly obtained by partitioning the composite-material distortional energy. The latter quantity is known, i.e. it is computed from the (known) composite-material deformation gradient and the effective shear modulus.

It should be also noted that in a general three-dimensional case the number of independent variables does not increase. However, the computational complexity increases since the stress deviator and the distortional energy of the composite material cannot be any longer related to the current density but rather have to be computed using the deformation gradient and the effective shear modulus.

*Numerical solution procedure.* In this section, a brief description is provided of the numerical procedure used to solve the set of nine equations identified in the previous section in order to determine the values of the nine associated composite-material and constituent state variables.

Among the nine equations identified in the previous section, seven are of an algebraic type while the remaining two (the two-constituent specific energy conservation equations (equation (12)) are of a (ordinary) differential character. Using a finite-differencing scheme, the latter two equations can be transformed into their incremental algebraic counterparts yielding a set of nine (non-linear) algebraic equations. These equations can be solved iteratively using a Newton-Raphson type numerical procedure. Anderson *et al.* (1990) has shown that this procedure can be greatly simplified by expressing the remaining dependent variables and their increments in terms of one of the constituents' volume fraction, e.g.  $\phi_1$  and its increment. Since the procedure proposed by Anderson *et al.* (1990) was used in the present work and it is fully described in Anderson *et al.* (1990), no further discussion of this procedure will be provided here.

---

*Implementation into a FEM code user-material subroutine.* As discussed earlier, within the commercial finite-element code environment, the user is allowed to implement a new material model (like the dynamic-mixture model, in the present case) through the use of a user-material subroutine. This was done in the present work in which, all the calculations were carried out using ABAQUS/Explicit finite-element package (ABAQUS, 2010). In the remainder of this section, a brief description is provided of the procedure used to implement the dynamic-mixture model into the VUMAT user-material subroutine of ABAQUS/Explicit.

Owing to the attendant large strains and rotations, the finite strain deformation formulation is adopted. Within this formulation, the basic quantity which relates/maps the original (homogenized) composite-material configuration into the current configuration is the deformation gradient,  $F$ . When material models like the one discussed here are implemented in user-material subroutines of the commercial finite-element codes, the (previous time and current time) deformation gradient and mass-densities are passed to the subroutine by the finite-element solver and the subroutine is tasked with computing and returning the corresponding composite-material stress state (as well as the values of all the material-state defining variables). The following quantities have been selected as the material-state variables:  $\phi_1$ ,  $P_1$ ,  $P_2$ ,  $\bar{E}_1$  and  $\bar{E}_2$ . The provided composite-material density is used in conjunction with  $\phi_1$  and  $\phi_2 = 1 - \phi_1$  to compute the corresponding constituent mass-densities. The latter are used in the EOS relations to obtain the constituent pressures via equation (10). One must also update the constituent energy densities via equation (12). The computation of the associated increments in the constituent energy densities requires the knowledge of the corresponding increments in distortional energy which, in turn, entails the calculation of the constituent deviatoric-strain increments. This is accomplished by first calculating the corresponding composite-material deviatoric-strain increment through the use of the previous and the current time deformation gradients and the standard definition of the logarithmic strain. Then the procedure outlined Appendix 1 is employed to first compute the associated composite-material deviatoric stress and the distortional-energy increment and then partition the latter quantity between the two constituents. At this point, the procedure proposed by Anderson *et al.* (1990) is employed to both update the composite-material stress state and energy as well as to update the aforementioned state variables. Most of the steps outlined above closely follow the ones used in our recent work (Grujicic *et al.*, 2011b).

## 2.2 Application to isotropic MMCs

The dynamic-mixture model overviewed in the previous section is applied in this section to a class of MMCs reinforced with micron-size ceramic particulates. The class of MMCs in question is typically fabricated using a pressure-less infiltration process (Rao and Jayaram, 2001) and, hence, is not expected to contain significant extents of elastic or plastic anisotropies. Consequently, the material will be treated as being isotropic and, due to a small size of the particulates, the homogenization assumption utilized within the dynamic-mixture method appears justified. In our previous work (Grujicic *et al.*, 2011a), the response of this class of MMCs was analyzed only in the intermediate-to-high strength shock regime in which the material response can be assumed to be dominated by its hydrodynamic (e.g. pressure, density, etc.) quantities. Clearly when the hydrodynamic approximation is used, the contribution of the stress

deviator and its energy-conjugate strain (rate) is minimal and can be neglected. In sharp contrast, in the weak-shock regime which is analyzed in the present work, both the hydrodynamic/volumetric and deviatoric/distortional effects contribute to the overall response of the composite material.

Also in Grujicic *et al.*, 2011a, only the adiabatic thermal-energy exchange regime is analyzed. In the present work, the analysis is extended to the isothermal regime within which the two constituents residing at the same material point are allowed to exchange the thermal energy until thermal equilibrium is reached. The specific MMC grade analyzed in the present work consists of an aluminium-matrix (60 vol.%) and micron-size SiC particulates (the remainder). The functional forms of the constituent (as well as for the composite-material) EOS relations used in the present work are overviewed in Appendix 2. The corresponding relations for the dissipative-pressure,  $Q$ , used in the present work are presented in Appendix 3. The associated constituent and composite-material model parameters are summarized in Table I.

### 3. Results and discussion

#### 3.1 Composite-material (shock) Hugoniot relations

In this section, the main shock-Hugoniot relations for planar, uniaxial-motion (longitudinal) shock waves in an Al-matrix, SiC-particulate reinforced MMC are determined and briefly discussed. Since the behavior of shock waves is governed by the corresponding jump equations, the energy conservation equation was replaced with the corresponding form of the Rankine-Hugoniot (jump) equation, in the present shock-wave analysis. Both the adiabatic and the isothermal-energy exchange limits are considered.

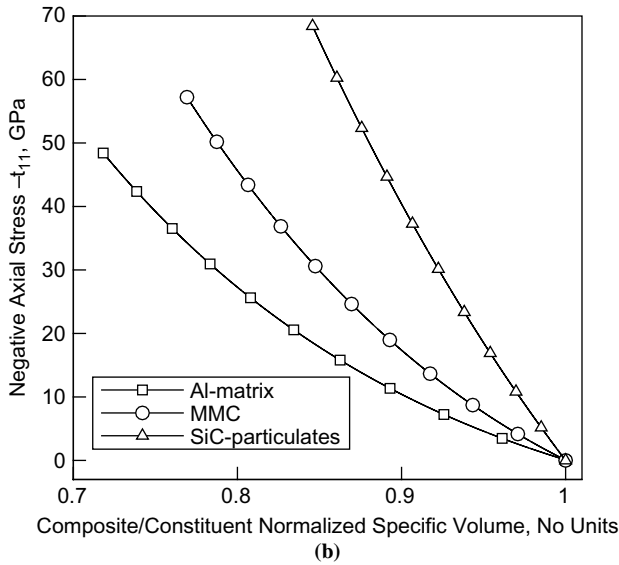
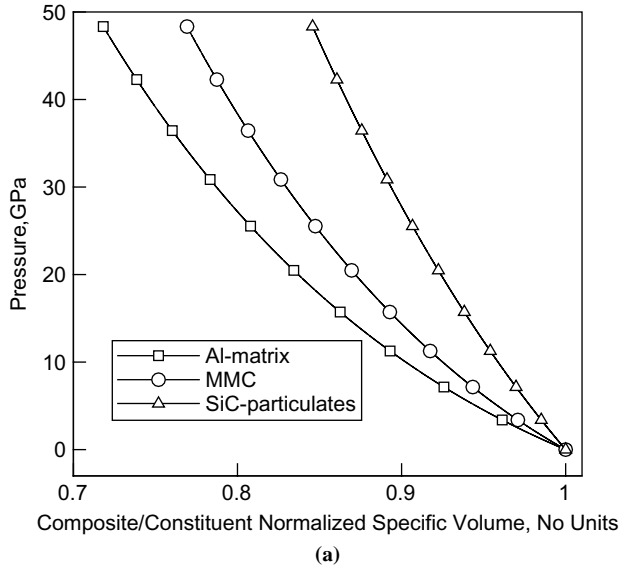
*Adiabatic limit.* Pressure ( $P$ ) vs ratio of the composite-material specific volume and the composite-material initial specific volume,  $v/v_0$ , shock-Hugoniot relation under adiabatic conditions is shown in Figure 1(a). The corresponding negative axial stress ( $-t_{11}$ ) vs  $v/v_0$  shock-Hugoniot relation is shown in Figure 1(b). For comparison, the corresponding  $P$  vs  $v/v_0$  and  $-t_{11}$  vs  $v/v_0$  relations are displayed for the two MMC constituents. In this case,  $v/v_0$  values pertain to the actual values of  $v/v_0$  in the composite-material and its constituents when the composite-material and its constituents are subjected to a constant-pressure level  $P$ . In other words, Figure 1(a)

Parameter	Units	Aluminum	SiC	MMC
$\rho_R$	kg/m <sup>3</sup>	2,785	3,215	2,805
$\Gamma_R$	–	2.0	1.56	1.89
$C_0$	m/s	5,328	N/A	N/A
$S$	–	1.338	N/A	N/A
$A_1$	GPa	N/A	220	88
$A_2$	GPa	N/A	361	171
$A_3$	GPa	N/A	0	120
$k_1$	–	1.2	1.2	1.2
$k_2$	–	0.06	0.06	0.06
$C_p$	J/kg K	870	800	–

**Table I.**

A summary of the material parameters for aluminum, SiC reinforcements and Al + SiC MMC

**Note:** See Appendix 1 for details



**Notes:** (a) Pressure vs normalized specific volume;  
 (b) negative axial stress vs normalized specific volume relations in the adiabatic thermal-energy exchange limit for an Al-40 vol.% SiC-particulate reinforced MMC; for comparison the corresponding normalized specific volumes for the composite-material constituents at the same level of pressure/stress are also depicted

**Figure 1.**  
Compressive-loading Hugoniot

shows that at any pressure level, the more volumetrically compliant aluminium-matrix undergoes significantly higher compression than the volumetrically stiffer SiC. Examination of the results shown in Figure 1(a) and (b) reveals that:

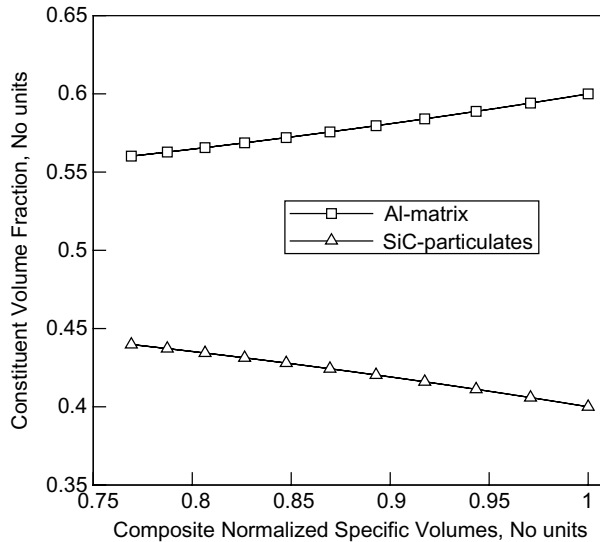
- As pointed above, compression is unequally distributed between the two constituents.
- A comparison of the constituent  $P$  vs  $v/v_0$  curves for the constituents with their respective shock-Hugoniot plots established that these two sets of curves are identical. This is not a surprise since in the adiabatic limit the composite-material  $P$  vs  $v/v_0$  curve is essentially obtained by application of dynamic rule of mixtures to the constituent  $P$  vs  $v/v_0$  Hugoniot relations.
- The deviatoric axial stress makes a contribution to the total axial stress in the aluminium-matrix which increases up to the point of yielding (under the condition  $-t_{11,Al} = t_{11,HEL,Al} = 437$  MPa) and remains constant afterwards.

It should be noted that a very rudimentary (no strain hardening/no temperature dependence) model for plasticity was used. In the case of SiC, no plastic deformation takes place and, hence, the contribution of the deviatoric stress to the total stress in SiC continuously increases with compression.

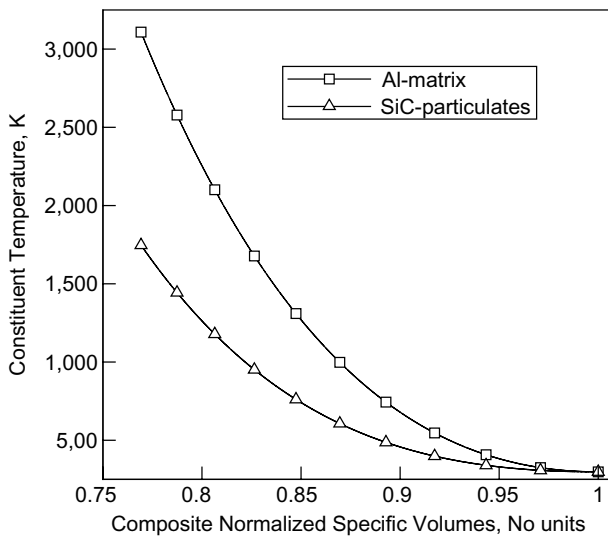
As mentioned above, the Hugoniot curves like the  $-t_{11}$  vs  $v/v_0$  curve in Figure 1(b) represent the *locus* of final (shock-strength dependent)/shock states but they do not represent the loading path/trajectory of the material points swept by the shock. Instead, it is the straight line (the Rayleigh line) in the  $-t_{11}$  vs  $v/v_0$  plot, which connects the initial/pre-shocked ( $v/v_0 = 1$  and  $-t_{11} = 0$ ) state and the final/post-shocked material state, that describes the loading path of the material particle as they are swept by the advancing shock-wave. The slope of the Rayleigh line is linearly related to the shock speed and will be used in this section to obtain a relationship between the shock speed and the particle velocity change brought about by the shock loading.

Variations in the volume fraction of the two constituents and their temperature with the shock strength, as quantified by the  $v/v_0$ , are shown in Figure 2(a) and (b), respectively. As expected, the volumetrically more compliant aluminum undergoes a reduction in its volume fraction (the opposite is true for the volumetrically stiffer SiC) (Figure 2(a)). This plot reveals the dynamic nature of the composite material when subjected to shock loading. Figure 2(b) shows that, as expected, the constituent which undergoes more compression and, thus, dissipates more energy during shock loading sustains a greater temperature increase. Since the two constituents residing at the same material point do not exchange thermal energy, a single temperature for the composite material cannot be defined in this case. The results shown in Figure 2(b) further suggest that the aluminium-matrix would undergo melting when subjected to strong shock loading. Since this type of phase transformation would modify the Al-matrix Hugoniot relations and, in turn, the MMC Hugoniot relations, the results shown in Figures 1 and 2 are not applicable at temperatures exceeding the melting point of aluminum.

*Isothermal limit.* Pressure ( $P$ ) vs  $v/v_0$  and  $-t_{11}$  vs  $v/v_0$  shock-Hugoniot relations for the composite material under isothermal conditions are shown, respectively, in Figure 3(a) and (b). For comparison, the corresponding  $P$  vs  $v/v_0$  and  $-t_{11}$  vs  $v/v_0$  relations are displayed for the two MMC constituents. Examination of the results shown in Figure 3(a) and (b) reveals that:



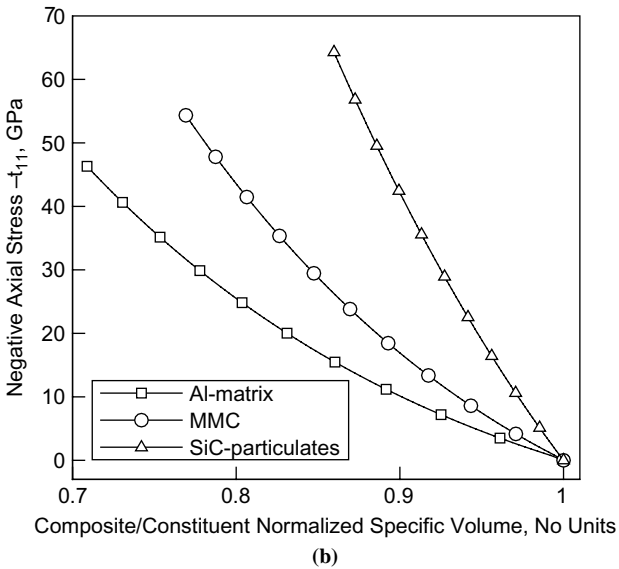
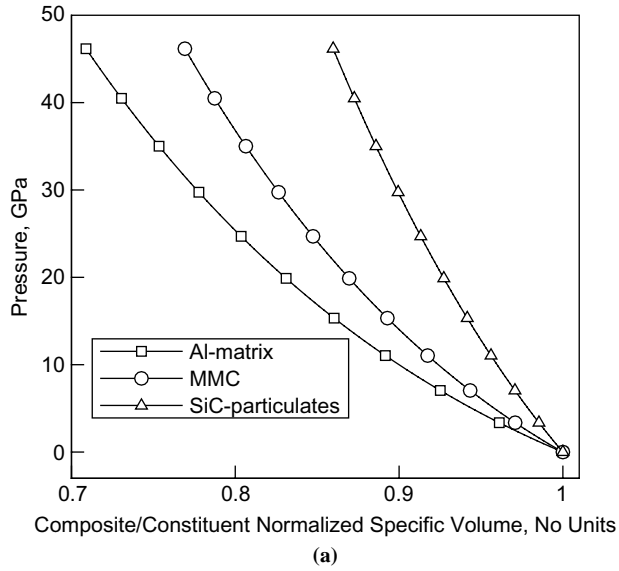
(a)



(b)

**Figure 2.** Variations of (a) constituent volume fraction; and (b) constituent temperature as a function of the composite-material normalized specific volume during compressive shock-based loading in the adiabatic thermal-energy exchange limit for an Al-40 vol.% SiC-particulate reinforced MMC

- At any pressure level, the more volumetrically compliant Al-matrix undergoes significantly higher compression than the volumetrically stiffer SiC.
- A comparison of the  $P$  vs  $v/v_0$  curves for the constituents with their respective shock-Hugoniot plots established that these two sets of curves are not any longer identical. This finding might be explained in the following way: Hugoniot



**Notes:** (a) Pressure vs normalized specific volume; (b) negative axial stress vs normalized specific volume relations in the isothermal thermal-energy exchange limit for an Al-40 vol.% SiC-particulate reinforced MMC; for comparison the corresponding normalized specific volumes for the composite-material constituents at the same level of pressure/stress are also depicted

**Figure 3.**  
Compressive-loading  
Hugoniot

relations are generally derived by combining the EOS with the Rankine-Hugoniot jump equation while assuming that no deposition of external energy or thermal-energy transport takes place. This condition is clearly not met in the isothermal limit where in order for the two constituents to attain thermal equilibrium, they must exchange (thermal) energy. In other words, in the present case, the Rankine-Hugoniot equation for the constituents contains an additional thermal-energy exchange term. The magnitude of this term is equal while the sign is opposite in the two constituents. Thus, the  $P$  vs  $v/v_0$  curves for the constituents shown in Figure 3(a) are the result of combining the appropriate EOS with the modified Rankine-Hugoniot equation.

- A comparison of the composite-material  $P$  vs  $v/v_0$  results shown in Figure 3(a) with those in Figure 1(a) shows that the pressure, at a constant-level of composite-material density, is slightly smaller in the isothermal than in the adiabatic case. This finding can be attributed to the higher value of  $\Gamma_{R\rho_R}$  in aluminum ( $= 5,709 \text{ kg/m}^3$ ) than in SiC ( $= 5,015 \text{ kg/m}^3$ ). Since  $\Gamma_{R\rho_R}$  represents the rate of change of pressure with a change in the internal energy, any transfer of energy from the higher-temperature aluminum to the lower temperature SiC will cause a larger drop of pressure in aluminum than the increase of pressure in SiC.
- As in the adiabatic case, the deviatoric axial stress makes a contribution to the total axial stress in the aluminium-matrix, but increases only to the point of yielding and remains constant thereafter. In sharp contrast, due to the absence of plasticity in SiC, this contribution continues to increase with compression.

Variations in the volume fraction of the two constituents and the composite-material temperature (the constituent temperatures and the composite-material temperature are now equal) with the shock strength, as quantified by the  $v/v_0$ , are shown in Figure 4(a) and (b), respectively. As expected, the volumetrically more compliant aluminum undergoes a reduction in its volume fraction while the volume fraction of the volumetrically stiffer SiC increases (Figure 4(a)). These results are very similar to their adiabatic counterparts shown in Figure 2(a). This finding is reasonable since, as shown above,  $\Gamma_{R\rho_R}$  values are not significantly different in the two composite-material constituents.

Figure 4(b) shows that the temperature of the composite material increases during loading (since shock loading is an energy-dissipative process) and that the magnitude of this increase scales with the shock strength (as quantified by deviation of the  $v/v_0$  parameter from unity). A comparison of the results shown in Figures 2(b) and 4(b) shows that the composite-material temperature, in the isothermal case, is roughly half-way between the constituent temperatures, in the adiabatic case. This finding is consistent with the fact that the aluminum-matrix and SiC-particulate reinforcement share comparable constant-pressure specific heats (Table I).

### 3.2 Analysis of the isentropic-decompression relations

In the previous section, the key shock-loading Hugoniot relations were presented and discussed for the subject Al-matrix, 40 vol.% SiC-particulate reinforced MMC and its constituents. As will be discussed in greater detail in the next section, decompression (centered simple) waves which form during reflection of the compression shocks from the free surface may pose a substantial threat to the target structure (and lead to

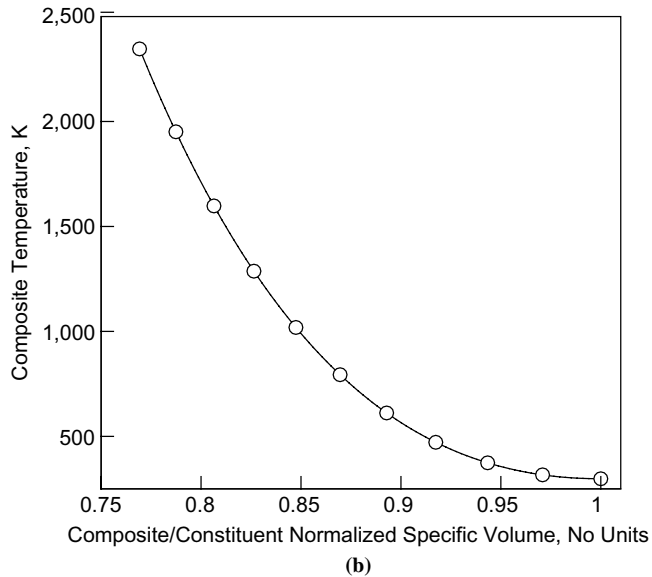
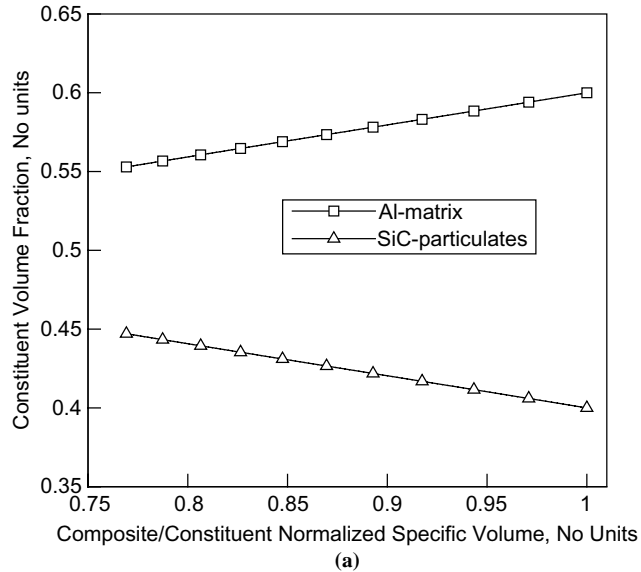
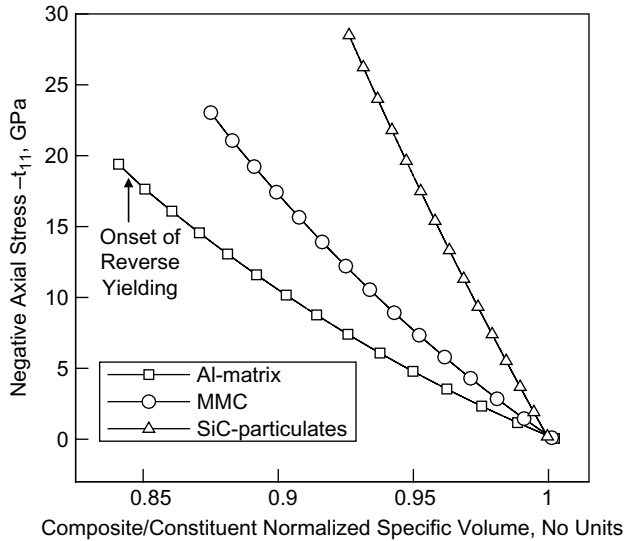


**Figure 4.** Variations of (a) constituent volume fraction; and (b) composite-material temperature as a function of the composite-material normalized specific volume during compressive shock-based loading in the isothermal thermal-energy exchange limit for an Al-40 vol.% SiC-particulate reinforced MMC

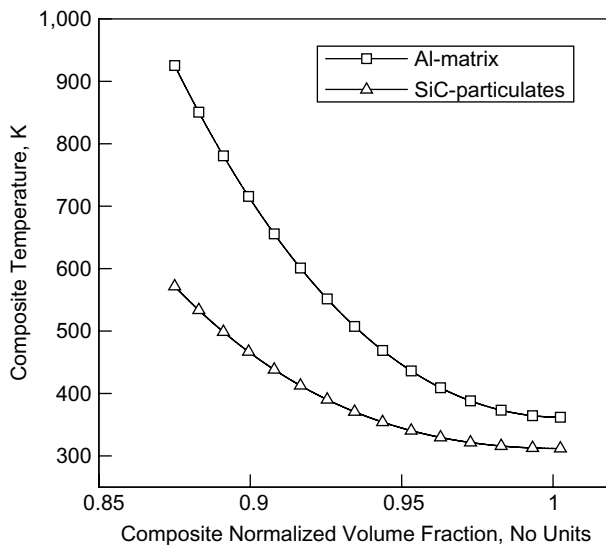
fracture mode commonly referred to as “spallation”). This is the reason that decompression relations of the subject MMC are investigated in present work. In all the analyses presented in this section, it will be assumed that the MMC was first shock compressed to a density which is 12.5 percent higher than its initial density. This is approximately the maximum compression to which the MMC can be subjected during shock loading before aluminum-matrix incipient melting takes place. Also, it will be assumed that subsequent unloading is of an isentropic character (i.e. free of energy

dissipative processes). As in the previous section, both thermal-energy exchange limits will be analyzed.

*Adiabatic limit.* The negative axial stress vs composite-material normalized specific volume isentropic-decompression relation under the adiabatic thermal-energy exchange condition for the subject MMC is shown in Figure 5(a). For comparison, the normalized specific volumes for the two constituents at the same level of pressure are also depicted in this figure. The corresponding constituent temperature vs



(a)



(b)

**Figure 5.**  
 (a) Isentropic decompression pressure vs normalized specific volume relation in the adiabatic thermal-energy exchange limit for an Al-40vol.% SiC-particle reinforced MMC; for comparison the corresponding normalized specific volumes for the composite-material constituents at the same level of pressure/stress are also depicted; and (b) the corresponding constituent temperature vs composite material normalized specific volume; the initial shock-induced compression (measured as an increase in the composite-material density) was 30 percent

composite-material normalized, specific-volume, isentropic-decompression relation for the subject MMC is shown in Figure 5(b). Examination of the results shown in Figure 5(a) and (b) reveals:

- Upon complete unloading ( $-t_{11} = 0$ ), the composite-material volume is greater than the initial volume (Figure 5(a)). This is simply the result of the fact that the residual composite-material temperature is higher than the initial temperature due to the fact that shock loading was associated with pronounced energy dissipation (temperature increase). In other words, shock-compression induced heating could not be fully reversed by isentropic-decompression induced cooling. This temperature increase leads to a positive (thermal) volumetric strain.
- Figure 5(a) also shows that the residual thermal-expansion effects are more pronounced in the aluminium-matrix than in SiC-particulates. This finding is consistent with the fact that volumetrically more compliant aluminum was substantially more compressed (and dissipated more energy) during shock loading than SiC.
- The local slope of the pressure vs  $v/v_0$  isentropic-decompression curve can be used to calculate the associated wave speed. This information, as will be discussed in greater detail in the next section, is a critical input into the analysis of propagation, reflection and interaction of decompression centered simple waves (CSWs) (Davison, 2008).
- In accordance with the previously observed larger thermal-expansion effects in Al, Figure 5(b) shows that the residual temperature in aluminum-matrix (ca. 370 K) is substantially higher than that in SiC-particulate reinforcements (ca. 310 K). It should be recalled that, as discussed earlier, in the adiabatic limit the temperature of the constituents may be determined, but the composite-material temperature is not defined.

Careful examination of the negative axial stress vs normalized specific volume plot for the aluminium-matrix, Figure 5(a), shows that this material initially decompresses elastically until the condition for reverse plastic yielding is attained. Beyond this point, further decompression of the aluminium-matrix involves distortional reverse plastic yielding and elastic volumetric unloading.

*Isothermal limit.* Negative axial stress vs composite-material normalized, specific-volume, isentropic-decompression relation under the isothermal thermal-energy exchange condition for the subject MMC is shown in Figure 6(a). For comparison, the normalized specific volumes for the two constituents at the same level of pressure are also depicted in this figure. The corresponding composite-material temperature vs composite-material normalized, specific-volume, isentropic-decompression relation is shown in Figure 6(b). In this case, the constituent temperatures are equal to the composite-material temperature at a given level of composite-material normalized specific volume. Examination of the results shown in Figure 6(a) and (b) reveals:

- As in the adiabatic case, the composite-material residual volume is larger than the initial volume (Figure 6(a)). This is again the result of the accompanying thermal-expansion effects. A comparison of the results shown in Figures 5(a) and 6(a) shows that under the isothermal condition, the thermal-expansion effects in the composite-material are somewhat less pronounced. This finding is

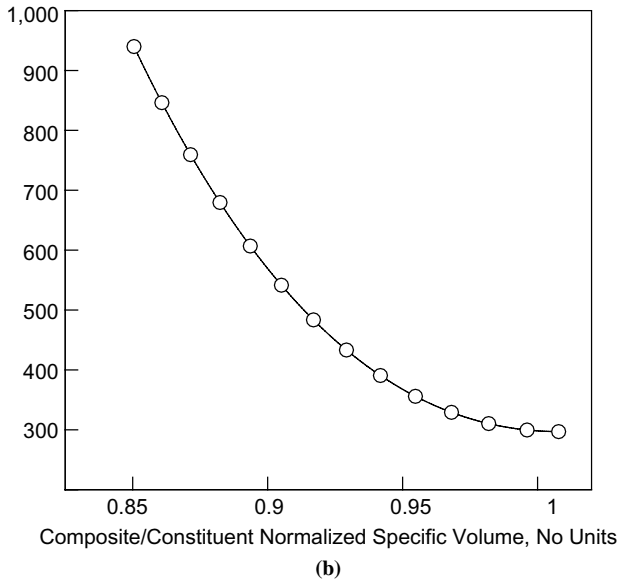
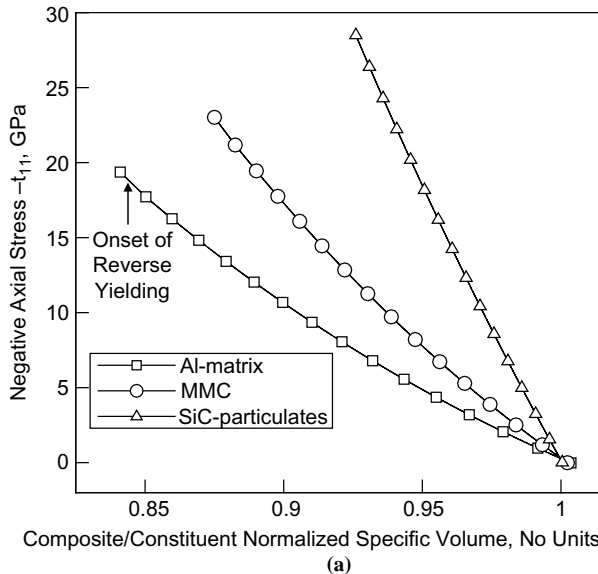


**Figure 6.**  
 (a) Isentropic decompression pressure vs normalized specific volume relation in the isothermal thermal-energy exchange limit for an Al-40vol.% SiC-particulate reinforced MMC; for comparison the corresponding normalized specific volumes for the composite-material constituents at the same level of pressure/stress are also depicted; and (b) the corresponding constituent temperature vs composite material normalized specific volume; the initial shock-induced compression (measured as an increase in the composite-material density) was 30 percent

consistent with the fact that the room-temperature thermal-expansion coefficient of aluminum (ca.  $22 \times 10^{-6}/K$ ) is roughly four times larger than its counterpart in SiC (ca.  $5 \times 10^{-6}/K$ ) and that the thermal-energy exchange under isothermal condition gives rise to quite comparable magnitudes (but opposite signs) of the Al-matrix and SiC-particulate reinforcement temperature changes. Thus, the resulting residual thermal expansion in the Al-matrix in the isothermal case

(relative to the adiabatic case) cannot be compensated by the associated increased thermal expansion in SiC-particulate reinforcements.

- As in the adiabatic case and for the same reason, the residual thermal-expansion effects are more pronounced in the aluminium-matrix than in SiC-reinforcements (Figure 6(a)).
- The local slope of the pressure vs  $v/v_0$  isentropic-decompression curve can be used to calculate the associated wave speed and then input into the analysis of propagation, reflection and interaction of simple waves.
- Figure 6(b) shows that upon complete decompression there is a residual temperature of ca. 316 K in the composite-material which is, as expected, between the Al-matrix and the SiC-particulate temperatures in the adiabatic case.

### 3.3 Analysis of intersecting isentropic-decompression smooth-waves

In the previous two sections, the dynamic-mixture theory was used to derive shock-loading Hugoniot and isentropic-unloading relations for a prototypical MMC. In the present section, it is demonstrated how these relations can be employed in the analysis of shock generation and propagation, and decompression/release wave generation, propagation and their interactions which may lead to the fracture mode commonly referred to as “spallation”.

A schematic of the problem analyzed here is shown in Figure 7. The problem analyzed is normally referred to as a flyer-plate impact problem. In this problem, a plate-like projectile moving at a constant velocity (referred to here as the projectile velocity) is allowed to impact a plate-like target. When the projectile and the target are made of the same material, the problem is referred to as a symmetric flyer-plate impact problem.

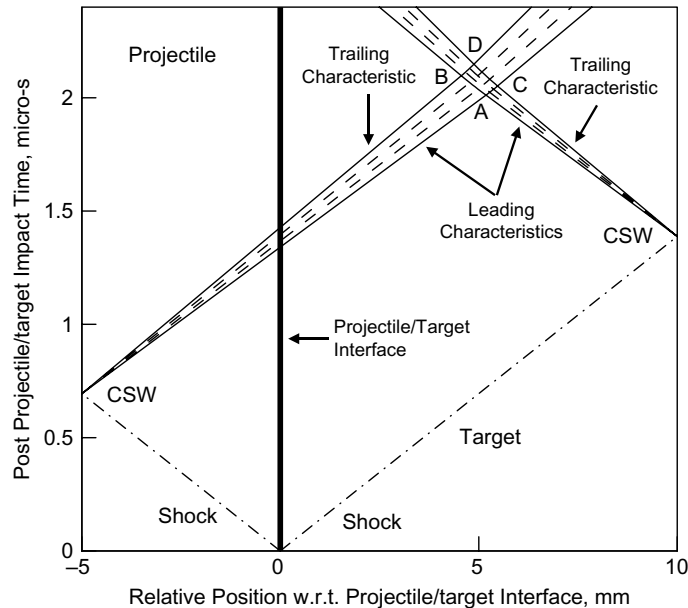


**Figure 7.** Characteristics-based Lagrangian-framework analysis of a symmetric flyer-plate impact problem in an Al-40 vol.% SiC-particulate reinforced MMC; the projectile initial velocity is 800 m/s; the required Hugoniot and isentropic relations used were those from the adiabatic thermal-energy exchange regime

This is the type of the flyer-plate impact problem analyzed in the present section. In addition, in the problem analyzed here, the thickness of the projectile is assumed to be smaller than the thickness of the target. Consequently, as will be shown below, spallation fracture may occur in the target plate.

The outcome of the flyer-plate impact problem analyzed here is shown in Figure 7, in which, time ( $t$ ) is cross-plotted against the spatial coordinate ( $X$ ) within the Lagrangian (material based) framework. As seen in Figure 7, upon impact, two shock waves are generated at the projectile/target interface. While one of the shock waves propagates to the left within the projectile, the other advances to the right within the target. Upon the reflection of the two shock waves from their respective (projectile or target back faces/free surfaces), two converging CSWs form. The right propagating CSW forms at the back face of the projectile, while a left propagating CSW forms at the target back face. As will be shown later, the intersection of these two waves results in the formation of a region within the target which is subjected to tensile stresses. If these tensile stresses are of sufficient magnitude, they may lead to spallation fracture.

Based on this description, the analysis presented in the remainder of this section is divided into three parts:

- (1) the analysis of formation and propagation of the shock waves;
- (2) the analysis of formation and propagation of the CSWs; and
- (3) the intersection of the two CSWs and the formation of the tensile regions within the target.

It should be also noted that a more detailed treatment of this problem will be addressed in our future work. Hence, the discussion presented in the remainder of this section is focused on the physics/conceptual aspects of the problem.

*Initial state of the projectile/target materials.* The material within the target is assumed to be initially quiescent ( $\dot{x}_T^- = 0$ , deformation-free  $\Delta^- = 0$  and stress-free  $t_{11}^- = 0$ ). The state of the material within the projectile is assumed to be the same as that within the target except that the initial particle velocity is equal to the projectile velocity ( $\dot{x}_p^- = 800$  m/s). It should be noted that in order to treat deformation of the projectile and the target in a consistent manner, Lagrangian compression ( $\Delta = 1 - \rho_R/\rho$ ) is used as a measure of the material deformation. The initial thicknesses of the projectile and the target are selected as  $L_p = 5$  mm and  $L_T = 10$  mm, respectively.

*Formation and propagation of incident shocks.* Owing to the symmetric nature of the flyer-plate impact problem, both the right and the left-propagating shocks produce a change in the particle velocity equal to one half of the projectile initial velocity. This change in the particle velocity is a measure of the shock strength. According to the standard physics-based analysis of planar longitudinal shocks (Davison, 2008), the changes in the remaining material states (e.g. axial stress/pressure, density, entropy density, etc.) can be computed provided one of the material shock-Hugoniot relations is known. In the present work, the axial stress vs normalized specific volume relations derived through the use of the dynamic-mixture theory, Figure 1(b), for the adiabatic case and, Figure 3(b), for the isothermal case, are used as the required shock-Hugoniot material relations. Thus, the dynamic mixture-based  $-t_{11}$  vs  $v/v_0$  relations enable complete determination of the material state behind the diverging shocks in the target and in the plate. It should be also noted that, in the shock regime, continuity in the particle velocity and in the axial stress is maintained across the projectile/target interface.

The procedure outlined above for the shock of a given strength (as controlled by the flyer-plate impact velocity) yields the associated values of the shock speed and the particle velocity. When this procedure is repeated for a range of flyer-plate impact velocity, a relationship between the shock speed and particle velocity can be obtained. The results of this procedure are shown in Figure 8 for the adiabatic and isothermal thermal-energy exchange regimes. A close examination of the results displayed in this figure reveals that, in each thermal-energy exchange case, there are two distinct branches (and a transition between the two) in the shock speed vs particle-velocity relation. The low particle-velocity branch is associated with elastic loading while the high particle-velocity branch is associated with elastic-plastic loading. Depending on the magnitude of particle velocity, the following three shock-wave regimes can be identified:

- (1) When the particle velocity falls in the range of the first branch, a single elastic-precursor shock is formed.
- (2) When the particle velocity falls in the transition region or on the second branch but the shock speed is lower than the maximum shock speed attainable in the first regime, two (a leading elastic-precursor and a trailing plastic) shock waves are formed.
- (3) When the particle velocity is high enough that the shock speed is higher than the maximum shock speed attainable in the first regime, a single elastic/plastic shock is formed. To simplify the analysis, only the case of a single elastic/plastic shock wave is considered here.

*Formation and propagation of CSWs.* Since the composite material under investigation is a so-called “normal” material, it supports the formation of shocks during compressive loading. Materials of this type, however, do not support the formation of shocks during unloading and, instead, smooth decompression CSWs are formed. Unlike shocks which bring about an abrupt/discontinuous change in the material

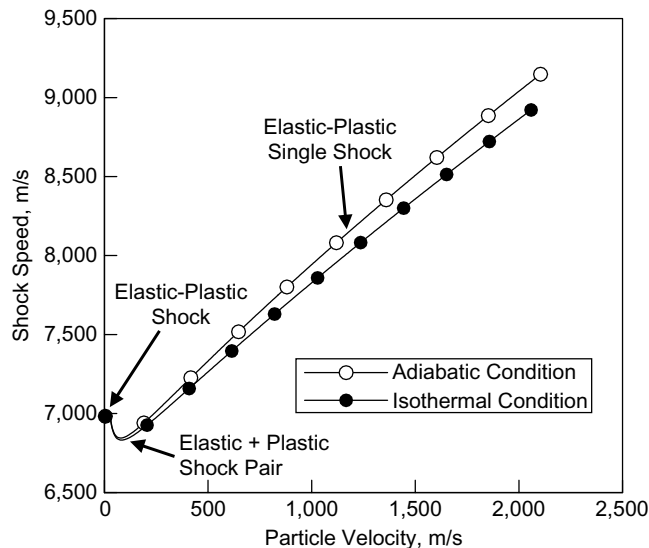


**Figure 8.** Shock speed vs particle velocity Hugoniot relation for an Al-40 vol.% SiC-particle reinforced MMC in the adiabatic and isothermal thermal-energy exchange conditions

states, CSWs give rise to a gradual/continuous change of these states between their levels ahead of the wave to their levels behind the wave. The head of the CSW is represented by a so-called “eading characteristic/wavelet”, while its tail is represented by the “trailing characteristic/wavelet”. The remaining interior portion of the CSW is defined in terms of the intermediate characteristics/wavelets. Each of these wavelets propagates through the material at a (compression-dependent) wave speed. In normal materials, the wave speed increases with the extent of material compression. This is the reason that, in normal materials, the leading characteristic which borders the fully compressed material advances at higher speeds than the trailing characteristic (borders the fully decompressed material) and that a shock wave cannot be formed during decompression.

According to the basic theory of CSWs (Davison, 2008), the CSW characteristics (before the two CSWs intersect) are each associated with the constant level of the wave speed and, hence, they appear as straight lines in the  $t$  vs  $X$  plot (Figure 7). The slope of each of these lines is equal to the reciprocal of the respective wave speed. Hence, to construct these lines a functional relation is needed between the sound speed and the extent of material compression. This relation was obtained in the present work using the  $-t_{11}$  vs  $v/v_0$  isentropic-decompression data shown in Figure 5(a), for the adiabatic case, and in Figure 6(a), for the isothermal case and the standard definition of the Lagrangian sound speed as:

$$C_L = -\sqrt{\frac{1}{\rho_R} \left( \frac{dt_{11}}{d\Delta} \right)}.$$

The results of this procedure are shown in Figure 9. Also, the leading and the trailing (as well as the remaining intermediate “receding”) characteristics of the two

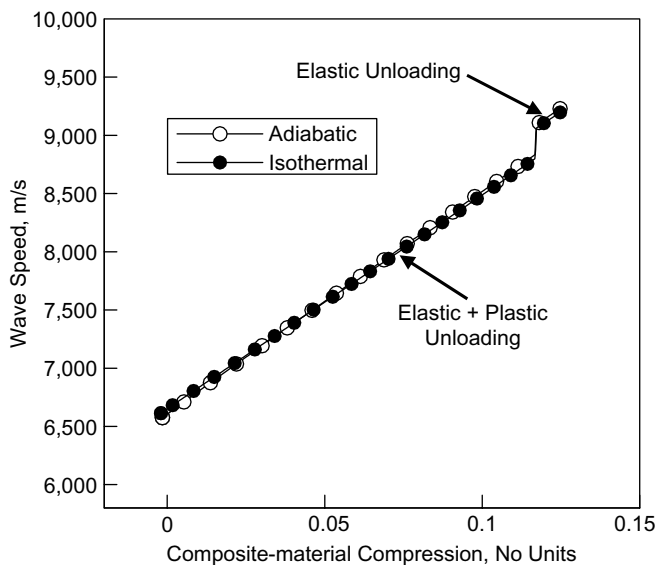


**Figure 9.** Wave speed vs particle velocity relation for isentropic decompression of an Al-40 vol.% SiC-particulate reinforced MMC in the adiabatic and isothermal thermal-energy exchange conditions

converging CSWs before, during and after their interaction, as shown in Figure 7, are constructed using these results (for the adiabatic case only).

Examination of the results shown in Figure 9 shows that the wave speed versus compression relations for both the adiabatic and the isothermal thermal-energy exchange conditions contains two distinct branches. The top branch is associated with the highest sound speed and corresponds to the initial elastic decompression of the aluminum-matrix and, in turn, to the elastic decompression of the entire composite material. This decompression ultimately produces a shear stress of sufficient magnitude and of a sign that is opposite to the shear stress accompanying loading. This results in the onset of reverse yielding. Thus, for the most part, unloading of the aluminum-matrix is the result of plastic decompression under a constant-level of the deviatoric/shear stresses and elastic unloading of the volumetric/hydrodynamic stress.

*Intersection of CSWs.* Examination of Figure 7 shows that ultimately the two CSWs will intersect within the target plate. The intersection/interaction region is denoted by four characteristic-intersection points:

- (1) the point *A* where the two leading characteristics intersect;
- (2) the points *B* and *C* where the leading characteristic of one wave intersects with the trailing characteristic of the other; and
- (3) the point *D* where the two trailing characteristics intersect.

It should be noted that the characteristics become curved (i.e. parabolic lines) within the interaction zone and subsequently become straight again once they have passed through the interaction region. To determine the shape of the CSW characteristics throughout the interaction region, the points of their intersection and the state of the material at these points, a method based on the concept of Riemann invariants (Davison, 2008), can be used. Details of this method are beyond the scope of the present work and will be presented in a future communication. An example of the results obtained through the application of this procedure is shown in Figure 10 in which temporal evolution of the negative axial stress at the spatial locations within the target corresponding to points *A*, *C* and *D* are depicted. Discontinuous/non-monotonic changes of  $-t_{11}$ , seen in Figure 10, are associated with either discrete events (e.g. arrival of a shock or a CSW) or with the transition of the material associated with the given point between different regimes of decompression, e.g. a transition of a material point from the single CSW regime to the interaction region and, in turn, into the post-interaction region. The results shown in Figure 10 show that, as a result of the intersection of the two CSWs, tensile stresses ultimately develop in the target. The location (or more precisely the plane) at which the tensile stress first attains a sufficiently high value (in combination with a probability of finding a potent material flaw or microstructural heterogeneity) will be the plane where the spallation initiates. In the present case, it is seen that points *A*, *C* and *D* are each associated with the largest tensile stress at different post-impact times. Hence, the magnitude of the failure strength and the stochastic nature of the flaws will dictate at which of these three locations (or a different location within the CSW interaction region) spallation cracking is more likely to occur. Once the initial spallation crack is formed, its subsequent growth in the lateral directions may result in incomplete separation of a layer of the target material at the target back face. As mentioned earlier, details of this process as well as those resulting from the formation of shocks at the spallation/crack faces will be presented in our future communication.

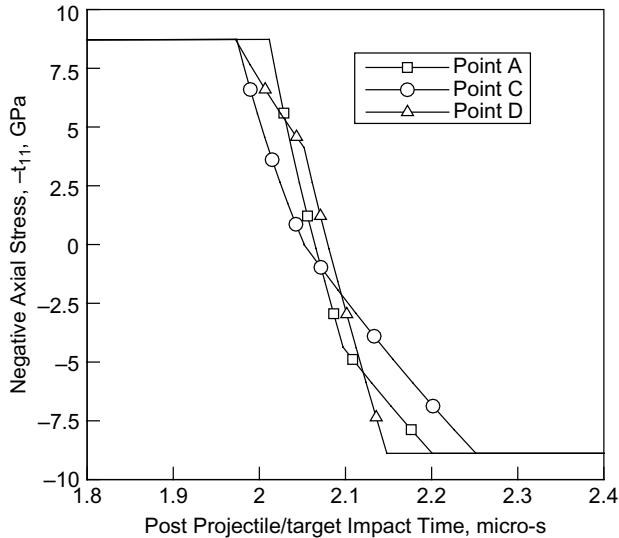


**Figure 10.** Temporal evolution of the negative axial stress at the spatial locations within the target corresponding to points A, C and D

#### 4. Summary and conclusions

Based on the results obtained in the present work, the following summary remarks and main conclusions can be drawn:

- In the present work, a critical assessment is carried out of the dynamic-mixture theory which is used to predict the behavior of natural and man-made mixtures under high-rate loading and unloading conditions.
- The theory is subsequently applied to a prototypical MMC material consisting of an aluminum-matrix and 40 vol.% SiC-particulate reinforcements. The application of the dynamic-mixture theory to the MMC material in question resulted in the generation of the appropriate loading Hugoniot and unloading-isentropic functional relations between various material-state variables. These were subsequently used to derive the corresponding shock speed vs particle velocity and smooth wave (characteristics) speed vs compression relations.
- In the last portion of the present work, the derived relations mentioned above are used to investigate the shock/wave phenomena resulting from the normal collision between a plate-like impactor and a plate-like target both made of the same MMC material. The analysis showed that the collision results in the formation of two diverging compression shock waves which, upon reflection from the projectile and the target free surfaces, become two converging decompression CSWs. The intersection of the two CSWs creates a region within the target plate which is subjected to tensile stresses. The combination of the tensile stress magnitude and the probability of finding a potent defect at a given location facilitates the formation of the so-called “spallation cracks”. Propagation of these cracks in the lateral directions produces a plate-like detachment/spall from the backside of the target-plate.

## References

- ABAQUS (2010), *Version 6.10, User Documentation*, Dassault Systems, Providence, RI.
- Abu Al-Rub, R.K. (2009), "Modeling the particle size and interfacial hardening effects in metal matrix composites with dispersed particles at decreasing microstructural length scales", *International Journal of Multiscale Computational Engineering*, Vol. 7 No. 4, pp. 329-50.
- Anderson, C.E., O'Donoghue, P.E. and Skerhut, D. (1990), "A mixture theory approach for the shock response of composite materials", *Journal of Composite Materials*, Vol. 4, pp. 1159-78.
- ANSYS/Autodyn-2D and 3D (2007), *Version 11, User Documentation*, ANSYS, Canonsburg, PA.
- Dang, P. and Gruzicic, M. (1997), "Transformation toughening in the gamma TiAl/beta Ti-V system – part II: a molecular dynamics analysis", *Journal of Materials Science*, Vol. 32, pp. 4875-87.
- Davis, J.R. (1993), *Aluminum and Aluminum Alloys*, 5th ed., ASM International, Materials Park, OH.
- Davis, J.R. (1997), *Heat Resistant Materials*, 2nd ed., ASM International, Materials Park, OH.
- Davison, L. (2008), *Fundamentals of Shock Wave Propagation in Solids*, Springer, Berlin.
- Drumheller, D.S. (1987), "Hypervelocity impact of mixtures", *International Journal of Impact Engineering*, Vol. 5, pp. 261-8.
- Gruzicic, M., Pandurangan, B., Bell, W.C., Yen, C.-F. and Cheeseman, B.A. *et al.* (2011a), "Application of a dynamic-mixture shock-wave model to the metal-matrix composite materials", *Materials Science & Engineering A*, Vol. 528 No. 28, pp. 8187-97.
- Gruzicic, M., He, T., Pandurangan, B., Runt, J., Tarter, J. and Dillon, G. (2011b), "Development and parameterization of a time-invariant (equilibrium) material model for segmented elastomeric polyureas", *Journal of Materials Design and Applications*, Vol. 225 No. 3, pp. 182-94.
- Hunt, E., Pitcher, P.D. and Gregson, P.J. (1990), *Preparation Reactions in 8090 Particulate Reinforced MMCs*, Technical Report ADA230646, Royal Aerospace Establishment, Bedford.
- Lee, I., Ochi, Y., Bae, S. and Song, J. (2009), "Continuum damage model for dynamic fracture toughness of metal matrix composites", *Journal of Solid Mechanics and Materials Engineering*, Vol. 3 No. 7, pp. 931-42.
- Li, Y., Ramesh, K.T. and Chin, E.S.C. (2007), "Plastic deformation and failure in A359 aluminum and an A359-SiC<sub>p</sub> MMC under quasi-static and high strain-rate tension", *Journal of Composite Materials*, Vol. 41 No. 1, pp. 27-40.
- Pandey, A.B., Kendig, K.L. and Watson, T.J. (2001), "Affordable metal matrix composites for high performance applications", *Proceedings of the TMS Materials Symposium, Indianapolis, IN, USA, November*.
- Rao, B.S. and Jayaram, V. (2001), "New technique for pressure-less infiltration of Al alloys into Al<sub>2</sub>O<sub>3</sub> preforms", *Journal of Materials Research*, Vol. 16 No. 10, pp. 2906-13.
- Vecchio, K.S. and Gray, G.T. (1994), "Shock-loading response of 6061-T6 aluminum-alumina metal matrix composites", *Journal de Physique III*, Vol. 4, pp. C8-231-C8-236.

## Appendix 1. Calculation of distortional power/energy

The energy conservation equation for the composite-material constituents, equation (12), contains a distortional power/energy term  $\rho_e \dot{E}_e^d$  which represents the rate at which the work is done by the

stress deviator while producing distortions within the composite-material constituent  $\varepsilon$ . The corresponding increase in the constituent distortional energy within a time increment  $\Delta t$  is denoted as  $\rho_\varepsilon \Delta E_\varepsilon^d$ . Within the dynamic mixture theory, the latter term is first evaluated for the composite material as a whole ( $\rho \Delta E^d$ ) and then partitioned between the constituents. This approach is justified by the fact that no relative motion is permitted between the constituents residing in the same material point. The  $\rho \Delta E^d$  term is evaluated as:

$$\rho \Delta E^d = (\Delta t) S_{\alpha\beta} \varepsilon_{\alpha\beta} \quad (A1)$$

where  $\varepsilon_{\alpha\beta}$  is the composite-material deviatoric strain rate and  $S_{\alpha\beta} \varepsilon_{\alpha\beta}$  is the volume-based, distortional power density. The composite-material deviatoric strain rate is evaluated from the known velocity gradient using standard kinematic relations. The corresponding stress deviator is then obtained using the appropriate version of the Hooke's law in the case of an elastic response or through the combined use of a yield criterion and a flow rule (in the case of an elastic-plastic response). In either case, the composite-material distortional-energy increment can be evaluated.

The composite-material distortional power/energy,  $\rho E^d$ , is then assumed to be partitioned between the constituents in the same way as the total internal energy, i.e. in accordance with equation (13). This yields the following form for the constituent distortional power/energy:

$$\rho_\varepsilon \Delta E_\varepsilon^d = \gamma_\varepsilon \rho \Delta E^d \quad (A2)$$

## Appendix 2. Equation of state

As mentioned in the main body of the manuscript, an EOS defines pressure dependence on density (i.e. degree of compression) and mass-based internal-energy density. In the present work, two forms of the EOS are used:

- (1) the so-called "shock" EOS for the aluminium-matrix (ANSYS/Autodyn-2D and 3D, 2007); and
- (2) the so-called "polynomial" EOS for the silicon carbide reinforcements (ANSYS/Autodyn-2D and 3D, 2007).

In addition, the MMCs are often modeled using the so-called "puff" EOS (ANSYS/Autodyn-2D and 3D, 2007).

It should be noted that subscript "epsilon" is omitted in this section to simplify notation. However, it will be clearly stated which relations apply to the constituents and which to the composite material as a whole. These three types of EOS can be generalized using the so-called "Mie-Gruneisen" EOS (Davison, 2008), which can be written as:

$$P(\mu) = P_R(\mu) + \Gamma_R \rho_R (E(\mu) - E_R(\mu)) \quad (A3)$$

where the compression is defined as  $\mu = 1 - \rho_0/\rho$  and the subscript "R" is used to define the reference curves/quantities.

### Shock EOS

In this case, the  $P_R(\mu)$  and  $E_R(\mu)$  are replaced with the corresponding Hugoniot curves,  $P^H(\mu)$  and  $E^H(\mu)$ , which are in turn defined using a linear  $U_s = C_0 + s\dot{x}$  relation ( $C_0$  and  $s$  are material constants) as:

$$P^H(\mu) = \frac{\rho_R C_0^2 \mu (1 + \mu)}{(1 - (s - 1)\mu)^2} \quad (A4)$$

$$E^H(\mu) = \frac{1}{2} \frac{P^H}{\rho_R} \left( \frac{\mu}{1 + \mu} \right) \quad (A5)$$

*Puff EOS*

In this case, the reference curves are again replaced with their respective Hugoniot curves. However, the latter are defined as:

$$P^H(\mu) = A_1\mu + A_2\mu^2 + A_3\mu^3 \quad (A6)$$

$$E^H(\mu) = \frac{P^H}{\rho_R} \left( \frac{\mu}{2} \right) \quad (A7)$$

where  $A_1$ ,  $A_2$  and  $A_3$  are material constants and equation (A7) is obtained from equation (A6) using the Rankine-Hugoniot relation and assuming that the initial pressure and energy in the material have zero-values.

*Polynomial EOS*

In this case,  $h_R = P_R(\mu) - \Gamma_R \rho_R E_R(\mu)$  appearing in equation (A3) is replaced with a third-order polynomial as:

$$h_R = A_1\mu + A_2\mu^2 + A_3\mu^3 \quad (A8)$$

Despite the fact that the Mie-Gruneisen EOS in the form of equation (A3) is often used, its physical-basis is generally overlooked. Equation (A3) simply states that, if a reference curve defined by functions  $P_R(\mu)$  and  $E_R(\mu)$  and lying on the  $P$ - $\rho$ - $E$  EOS surface is known, the EOS surface can be reconstructed in the neighborhood of the reference curve by expanding each point of the curve, at a given of  $\mu$  into a constant- $\mu$  line segment, so that the slope of this line segment is equal to  $\Gamma_R$  (the Gruneisen Gamma) material parameter.

A summary of the EOS material model parameters for the aluminium-matrix, SiC reinforcements and the Al + SiC MMC is given in Table I.

**Appendix 3. Dissipative pressure constitutive relation**

In accordance with the work of Anderson *et al.* (1990), the following constitutive relation is used for the constituent dissipative pressure,  $Q$  (subscript “epsilon” is again omitted), in the present work:

$$Q = \rho k_1^2 \left( \frac{\dot{\rho}}{\rho} \right)^2 + \rho k_2 C_0 \left| \frac{\dot{\rho}}{\rho} \right| = \rho (q_q + q_l) \quad (A9)$$

where  $k_1$  and  $k_2$  are material constants.

Clearly, since  $Q$  scales with  $\dot{\rho}/\rho$ , it can take significant values only in the shock front region where the rate of change of material density is significant.

A summary of the dissipative pressure material model parameters for the aluminium-matrix, SiC reinforcements and the Al + SiC MMC is given in Table I.

**About the authors**

M. Grujicic is a Professor of Mechanical Engineering in the Department of Mechanical Engineering, Clemson University. His research interests include computational engineering. M. Grujicic is the corresponding author and can be contacted at: gmica@clemson.edu

---

W.C. Bell is a PhD Student in the Department of Mechanical Engineering, Clemson University whose research interests include computational modelling and shock physics.

B. Pandurangan is a Post-doctoral Fellow, Mechanical Engineering, Clemson University, whose research interests include computational material modeling.

C-F. Yen is a Research Engineer at the Army Research Labs, Aberdeen Proving Ground, whose research interests include composite modeling.

B.A. Cheeseman is a Research Engineer at the Army Research Labs, Aberdeen Proving Ground, whose research interests include blast modeling and simulation.